A Heterogeneous Kinetics Model for Triplet Exciton Transfer in Solid-State Upconversion

A heterogeneous kinetics model for triplet exciton transfer in solid-state upconversion

Nadav Geva,[†] Lea Nienhaus,[‡] Mengfei Wu,[¶] Vladimir Bulović,[¶] Marc A. Baldo,[¶] Troy Van Voorhis,[,‡] and Moungi G. Bawendi[*,‡]*

†Department of Materials Science and Engineering, ‡Department of Chemistry, ¶Department of Electrical Engineering and Computer Science, Massachusetts Institute of Technology, Cambridge, MA 02139

*corresponding authors: tvan@mit.edu and mgb@mit.edu

ABSTRACT

High internal quantum efficiency semiconductor nanocrystal (NC)-based photon upconversion devices are currently based on a single monolayer of active NCs. Devices are therefore limited in their external quantum efficiency based on the low number of photons absorbed. Increasing the number of photons absorbed is expected to increase the upconversion efficiency, yet experimentally increasing the number of layers does not appreciably increase the upconverted light output. We unravel this mystery by combining kinetic modeling and transient photoluminescence spectroscopy. The inherent energetic disorder stemming from the polydispersity of the NCs means that the kinetics are governed by a stochastic transfer matrix. By drawing the rates from a probabilistic distribution and constructing a reaction network with realistic connectivity, we are able to fit complex photoluminescence traces with a very simple model. We use this model to explain the thickness-dependent performance of the upconversion devices, and can attribute the reduced efficiencies to the low excitonic diffusivity of the exciton within the NC layers and increased back transfer of the created singlets from the organic annihilator rubrene. We suggest some avenues for overcoming these limitations in future devices.

Keywords: upconversion efficiency, triplet exciton transfer, triplet-triplet annihilation, energetic disorder, nanocrystals

The hybrid interface between colloidal nanocrystals (NCs) and organic semiconductors (OSCs) provides new avenues in optoelectronic research.[1–6] By combining the tunable electronic structure of NCs with the unique features of OSCs, it is possible to engineer devices that can overcome the Shockley-Queisser[7] limit in single-junction photovoltaics,[8,9] improve biological imaging[10] and reduce the cost of infrared imaging.[11]

In contrast to non-linear frequency upconversion using lanthanide ions which requires high

photon fluxes,[11–13] the upconversion process here relies on direct triplet sensitization of the OSC (typically rubrene) and subsequent diffusion-mediated triplet-triplet annihilation (TTA). Taking advantage of the long-lived triplet states, this TTA-based process is viable at sub-solar photon fluxes.[14] TTA relies on the interaction of two spin-triplets on neighboring molecules, which can interact to generate a higher-lying spin-singlet excited state.[8,15,16] However, triplet states are spin-forbidden due to spin-selection rules and therefore not directly optically accessible: triplet sensitizers are required. Conventionally, this has been achieved by phosphorescent metal-organic complexes which show strong intersystem crossing.[15,17–19] Recently, lead sulfide (PbS) NCs have been shown to be efficient triplet sensitizers.[1,4,5,14,20] In particular, these devices take advantage of the rapid spin-dephasing in PbS semiconductor NCs resulting from the small exchange interaction between singlet and triplet states at the band edge caused by strong spin-orbit coupling.[21,22] This allows the NCs to directly sensitize the otherwise optically inactive spin-triplet states in the OSC by direct triplet exciton transfer (TET) from the band-edge exciton on the PbS NC. This TET process maintains the spin state, and is therefore an allowed transition.[23]

Recent progress on the up-conversion system composed of PbS NCs and rubrene has shown that the triplet exciton transfer at the inorganic-organic interface can be made fast and efficient, by tuning the ligand length separating the NC and rubrene.[4,24] However, so far focus has been placed on increasing the internal device efficiency: the percentage of absorbed low-energy photons which are converted into high-energy photons. The external upconversion efficiency, defined as the percentage of total converted incident photons, remains low. To achieve a high device efficiency, a larger fraction of incoming photons must be absorbed and subsequently transferred into the upconverting layer.

In our previous studies the main goal was to decipher the underlying TET mechanism, which is thought to be based on a short-range exchange-mediated energy transfer (Dexter mechanism).[4,5,25] To minimize effects caused by inter-dot energy transfer, the NC film thickness in the devices was limited to one monolayer (ML),[4] resulting in an achievable external upconversion efficiency well below 1%, due to the absorption of *ca.* 0.5% per ML PbS NCs at the first excitonic feature in the absorption spectrum.

In this work, we investigate the dependency of the upconversion efficiency on the NC film thickness, using an octanoic acid (8 C) ligand. This ligand length was chosen to decrease the inter-NC spacing, and promote increased exciton transport in the PbS NC film, yet avoid potential charge separation, as well as increase the TET rate due to the reduced NC-rubrene spacing.

When increasing the NC film thickness from one ML to two MLs (Figure 1a,b), to first-order approximation one would expect a doubling in the upconverted steady-state PL (Figure 1c), due to the fact that twice as many photons are absorbed by the NC film. As only excitons at the NC-OSC interface can undergo the short-range TET, this approximation is only valid if exciton transfer (ET) from the second ML is efficient to the interface.

We experimentally find that although the upconverted steady-state PL (corresponding to the external upconversion efficiency) increases slightly (~5% increase) going from one to two MLs (Figure 1d), the internal upconversion efficiency decreases by about half, since twice as many photons are absorbed in the case of two MLs. This indicates that ET from the second NC ML to the first NC ML is likely inefficient.

To investigate the underlying reason for this result, we turn to transient photoluminescence spectroscopy. Figure 2a shows the thickness dependent PL dynamics of the NC films in absence of rubrene (brown traces), as well as the quenched dynamics in presence of rubrene for one ML (green) and two MLs (red). Using the previously reported extraction method of active and inactive NCs, we obtain a population of 92% active NCs for the single ML NC device, and 49% active NCs for the two ML device. This result is in good agreement with the observed *ca.* 5% increase in the external upconversion efficiency seen in the steady-state PL, assuming the second ML does not play a large role in TET due to inefficient ET to the NC/rubrene interface.

However, the late-time PL decay dynamics, which can be associated with the inactive PbS NC fraction show an unexpected result: in the presence of rubrene, the NCs show a slower decay than their unperturbed counterparts. This can be seen in the non-parallelity of the late-time dynamics (Figure 2a, dashed black lines function as guides to the eye). This is consistent with a replenishment of the NC exciton population at later times, which we attribute to a back-transfer of the singlet excitons created by TTA. To model this, we construct a simple model of the process as shown in Figure 2b. The PbS NC population with an exciton lifetime of 2.4 μs (brown traces) is quenched by TET to rubrene with a time constant of 150 ns for one ML (green) and 2 ML (red). To account for the non-parallelity, the PbS NC population is replenished by singlet back transfer modeled with an estimated 15 μs lifetime of the diffusion-mediated TTA based triplet-singlet conversion in rubrene convoluted by the 2.4 μs inherent PbS NC lifetime (Figure 2b, bottom inset).

We can see that this simple model qualitatively reproduces the observed PL kinetics both in

presence and in absence of rubrene, yet it cannot capture the multi-exponential decay dynamics observed experimentally for the NC films. One anticipates that this multiexponential behavior results from the polydispersity of the NCs. In crystalline and highly ordered systems, PL decay dynamics can be easily fit by such a single exponential function. In a system with multiple decay channels or multiple populations with a variety of decay rates, the resulting dynamics can be highly multi-exponential.[26,27] The different rates can in principle be captured by a multi-exponential fit. Unfortunately, trying to fit a large number of exponentials to a single time trace is mathematically ill-posed. As a result, extracting more than two or three time constants simultaneously is experimentally very challenging.

For the hybrid NC-OSC system investigated here one can sidestep this issue to some extent by invoking an active/inactive PbS NC model to extract the TET decay dynamics – simply subtracting the multi-exponential decay dynamics of the "inactive" PbS NC population – and thereby extract overall efficiencies in the presence of disorder.[4,5] However, the transfer matrix formalism provides a more general solution, allowing us to describe the kinetics of a system with a true *distribution* of rates.[28] Below we briefly outline how this method is used to describe the kinetics of our devices, with more details provided in the Supporting Information.

There are four important processes in the model:

- **Nanocrystal PL rates** Each NC is assumed to have its own radiative decay rate (k_i). It is evident from the multiexponential nature of the PL data that these rates must be heterogeneous. We assume the decay rates follow a log-normal distribution, so that k_i for the i^{th} dot takes the form:

$$k_i = \bar{k} \exp\left(-\frac{\Delta E_i}{kT}\right)$$

  Where the effective energy barriers ΔE_i are normally distributed. The decay rates are thus governed by two parameters: the mean rate, $\bar{k}$, and standard deviation E_σ of the distribution of activation energy barriers.
- **NC-to-OSC Energy Transfer**. These rates (k_{TET}) are assumed to be zero for dots more than one layer separated from the OSC due to the short range nature of triplet energy transfer.[4,29,30]
- **NC-to-NC Energy Transfer** We model the energy transfer between NCs of different

sizes using the Bell-Evans-Polanyi principle:[31,32]

$$k_{NC}^{ET} = \begin{cases} \bar{k}^{ET} \exp\left(\frac{E_i - E_j}{kT}\right) & if\ E_j > E_i \\ \bar{k}^{ET} & if\ E_j \leq E_i \end{cases} \quad (5)$$

This results in preferential energy transfer from small NCs (higher energy) to large NCs (lower energy). The distribution of NC energies we use is a normal distribution fit, based on the known size polydispersity (2.67 ± 0.35 nm) of the NCs used here and the empirical equation by Moreels *et al*. linking the size and band gap of PbS NCs.[33]

- **OSC-to-NC Energy Transfer.** These rates (k_b) reflect the back transfer of upconverted singlet excitons to the NCs These rate constants are assumed to be nonzero for all dots in the device due to the longer-ranged nature of singlet energy transfer. [29,34]

This model captures the minimal physics required to quantitatively describe these devices. The NCs are assumed to occupy a hexagonal close-packed grid coupled to a bulk OSC phase on one side. We emphasize that this method is stochastic and the results are therefore averaged over a large set of rates – strictly analogous to the ensemble average in the experiment.

We used the above method to model the PL dynamics seen in Figure 2a. The main feature to note is the ability of this model to capture the "bendiness" of the PL curve (the degree to which the PL curve varies from linear on a semi-logarithmic scale, which denotes purely mono-exponential behavior). This effect is usually accounted for using a multi-exponential fit. However, if there is no *a priori* knowledge of multiple discrete populations present in the sample, it is hard to associate meaning with the fit parameters, and the number of parameters can quickly become unphysical. In the present model, a very non-linear curve is fit using only two parameters: the mean and energy variance of the decay constant. As can be seen in Figure 3b the model fits the data very well. As shown in the Supporting Information, a stretched exponential fits the 1ML data almost equally well, so the present result should not be seen as incontrovertible proof of the log-normal ansatz for k_i . Rather, this choice is one of several rate distributions that is consistent with the experimental data. As expected, both model and experiment show very little dependence of the infrared PL dynamics on the number of MLs. We note that the degree of heterogeneity, defined as the variance in the rate distribution, is quite small energetically, on the order of 37 meV. The interesting part comes in the measurement of the NCs with a rubrene layer. The model is able to reproduce both experimental curves with a single set of rate parameters.

Figure 4 summarizes the flow of energy in the system. The interfacial ML of PbS NCs can

efficiently couple to the rubrene and transfer energy. The additional second ML of NCs is too far from the NC-rubrene interface for TET to occur directly. Some ET from the second PbS NC ML to the interfacial ML does occur. According to the model the second layer enhances the forward flux by up almost 10%. But that flux is partly cancelled by an increase in the back transfer of upconverted singlets to the NCs. Basically, the additional MLs provide an additional source *and sink* for excitons and the two effects roughly cancel one another. Using the full kinetic model, we are also able to confirm that the late time deviation from parallelity is due to different rates of back-transfer. Indeed, careful observation of the long-time data is consistent with the notion that back transfer is more efficient in the two ML sample as compared to one, and the heterogeneous kinetics model correctly reproduces this result without any additional parameters.

In conclusion, we have presented a kinetic model which can capture the decay dynamics of disordered systems. We then applied the model to an upconverting system composed of NCs with an OSC phase, and deduced the relevant rate constants. We find that the model predicts a rapid decline in internal efficiency with increasing NC layer thickness due to inefficient inter-dot ET and rapid back transfer of the created singlet excitons. This back transfer may be the underlying cause of the only 7 % internal upconversion efficiency in the one ML devices, despite nearly unity TET efficiency.[4] To further increase the external upconversion efficiency, future work should first aim to increase the interdot ET efficiency while maintaining near unity TET. Our simulations suggest that most of the excitons in the second dot layer fail to make it into the rubrene layer, severely limiting device performance. A second aim is reducing the amount of back transfer of the upconverted singlets from the OSC to the NC layers, possibly by using energy funneling ideas.

AUTHOR INFORMATION

Corresponding Author

*Troy Van Voorhis: tvan@mit.edu

*Moungi G. Bawendi: mgb@mit.edu

ORCID

Lea Nienhaus: 0000-0003-1412-412X

Mengfei Wu: 0000-0002-4728-3234

Marc A. Baldo: 0000-0003-2201-5257

Moungi G. Bawendi: 0000-0003-2220-4365

Notes

The authors declare no competing financial interests.

ACKNOWLEDGMENTS

This work was primarily supported as part of the Center for Excitonics, an Energy Frontier Research Center funded by the US Department of Energy, Office of Science, Office of Basic Energy Sciences under Award Number DE-SC0001088 (MIT).

REFERENCES

(1) Huang, Z.; Li, X.; Mahboub, M.; Hanson, K. M.; Nichols, V. M.; Le, H.; Tang, M. L.; Bardeen, C. J. Hybrid Molecule–Nanocrystal Photon Upconversion Across the Visible and Near-Infrared. *Nano Lett* **2015**, *15* (8), 5552–5557.

(2) Piland, G. B.; Huang, Z.; Lee Tang, M.; Bardeen, C. J. Dynamics of Energy Transfer from CdSe Nanocrystals to Triplet States of Anthracene Ligand Molecules. *J Phys Chem C* **2016**, *120* (11), 5883–5889.

(3) Mongin, C.; Garakyaraghi, S.; Razgoniaeva, N.; Zamkov, M.; Castellano, F. N. Direct Observation of Triplet Energy Transfer from Semiconductor Nanocrystals. *Science* **2016**, *351* (6271), 369.

(4) Nienhaus, L.; Wu, M.; Geva, N.; Shepherd, J. J.; Wilson, M. W. B.; Bulović, V.; Van Voorhis, T.; Baldo, M. A.; Bawendi, M. G. Speed Limit for Triplet-Exciton Transfer in Solid-State PbS Nanocrystal-Sensitized Photon Upconversion. *ACS Nano* **2017**, *11* (8), 7848–7857.

(5) Wu, M.; Congreve, D. N.; Wilson, M. W. B.; Jean, J.; Geva, N.; Welborn, M.; Van Voorhis, T.; Bulović, V.; Bawendi, M. G.; Baldo, M. A. Solid-State Infrared-to-Visible Upconversion Sensitized by Colloidal Nanocrystals. *Nat Photon* **2016**, *10* (1), 31–34.

(6) Wu, M.; Jean, J.; Bulović, V.; Baldo, M. A. Interference-Enhanced Infrared-to-Visible Upconversion in Solid-State Thin Films Sensitized by Colloidal Nanocrystals. *Appl. Phys. Lett.* **2017**, *110* (21), 211101.

(7) Shockley, W.; Queisser, H. J. Detailed Balance Limit of Efficiency of P-n Junction Solar Cells. *J Appl Phys* **1961**, *32* (3), 510–519.

(8) Schulze, T. F.; Schmidt, T. W. Photochemical Upconversion: Present Status and Prospects for Its Application to Solar Energy Conversion. *Energy Env. Sci* **2015**, *8* (1), 103–125.

(9) Trupke, T.; Green, M. A.; Würfel, P. Improving Solar Cell Efficiencies by Up-Conversion of Sub-Band-Gap Light. *J Appl Phys* **2002**, *92* (7), 4117–4122.

(10) Wu, X.; Chen, G.; Shen, J.; Li, Z.; Zhang, Y.; Han, G. Upconversion Nanoparticles: A Versatile Solution to Multiscale Biological Imaging. *Bioconjug. Chem.* **2015**, *26* (2), 166–175.

(11) Zhou, J.; Liu, Q.; Feng, W.; Sun, Y.; Li, F. Upconversion Luminescent Materials: Advances and Applications. *Chem Rev* **2015**, *115* (1), 395–465.

(12) Auzel, F. Upconversion and Anti-Stokes Processes with f and d Ions in Solids. *Chem. Rev.*

2004, *104* (1), 139–174.
(13) Chen, G.; Qiu, H.; Prasad, P. N.; Chen, X. Upconversion Nanoparticles: Design, Nanochemistry, and Applications in Theranostics. *Chem. Rev.* **2014**, *114* (10), 5161–5214.
(14) Mahboub, M.; Huang, Z.; Tang, M. L. Efficient Infrared-to-Visible Upconversion with Subsolar Irradiance. *Nano Lett* **2016**, *16* (11), 7169–7175.
(15) Singh-Rachford, T. N.; Castellano, F. N. Photon Upconversion Based on Sensitized Triplet–Triplet Annihilation. *Coord Chem Rev* **2010**, *254* (21–22), 2560–2573.
(16) Schmidt, T. W.; Castellano, F. N. Photochemical Upconversion: The Primacy of Kinetics. *J Phys Chem Lett* **2014**, *5* (22), 4062–4072.
(17) Monguzzi, A.; Tubino, R.; Meinardi, F. Multicomponent Polymeric Film for Red to Green Low Power Sensitized Up-Conversion. *J Phys Chem A* **2009**, *113* (7), 1171–1174.
(18) Amemori, S.; Sasaki, Y.; Yanai, N.; Kimizuka, N. Near-Infrared-to-Visible Photon Upconversion Sensitized by a Metal Complex with Spin-Forbidden yet Strong S0–T1 Absorption. *J Am Chem Soc* **2016**, *138* (28), 8702–8705.
(19) Trupke, T.; Shalav, A.; Richards, B. S.; Würfel, P.; Green, M. A. Efficiency Enhancement of Solar Cells by Luminescent Up-Conversion of Sunlight. *Sol Energ Mat Sol Cells* **2006**, *90* (18–19), 3327–3338.
(20) Nienhaus, L.; Wu, M.; Bulovic, V.; Baldo, M. A.; Bawendi, M. G. Using Lead Chalcogenide Nanocrystals as Spin Mixers: A Perspective on near-Infrared-to-Visible Upconversion. *Dalton Trans.* **2018**.
(21) Kim, J.; Wong, C. Y.; Scholes, G. D. Exciton Fine Structure and Spin Relaxation in Semiconductor Colloidal Quantum Dots. *Acc Chem Res* **2009**, *42* (8), 1037–1046.
(22) Scholes, G. D.; Rumbles, G. Excitons in Nanoscale Systems. *Nat Mater* **2006**, *5* (9), 683–696.
(23) You, Z.-Q.; Hsu, C.-P. Theory and Calculation for the Electronic Coupling in Excitation Energy Transfer. *Int J Quantum Chem* **2014**, *114* (2), 102–115.
(24) Geva, N.; Shepherd, J. J.; Nienhaus, L.; Bawendi, M. G.; Van Voorhis, T. Morphology of Passivating Organic Ligands around a Nanocrystal. **2017**, arXiv:1706.00844 [physics.chem–ph] arXiv.org e–Print archive. https://arxiv.org/abs/1706.00844 (accessed Jun 5, 2017).
(25) Dexter, D. L. A Theory of Sensitized Luminescence in Solids. *J Chem Phys* **1953**, *21* (5), 836–850.
(26) Resch-Genger, U.; Grabolle, M.; Cavaliere-Jaricot, S.; Nitschke, R.; Nann, T. Quantum Dots versus Organic Dyes as Fluorescent Labels. *Nat. Methods* **2008**, *5*, 763.
(27) Fisher, B. R.; Eisler, H.-J.; Stott, N. E.; Bawendi, M. G. Emission Intensity Dependence and Single-Exponential Behavior In Single Colloidal Quantum Dot Fluorescence Lifetimes. *J. Phys. Chem. B* **2004**, *108* (1), 143–148.
(28) Marin, G.; Yablonsky, G. S. *Kinetics of Chemical Reactions*; John Wiley & Sons, 2011.
(29) Scholes, G. D. LONG-RANGE RESONANCE ENERGY TRANSFER IN MOLECULAR SYSTEMS. *Ann Rev Phys Chem* **2003**, *54* (1), 57–87.
(30) Thompson, N. J.; Wilson, M. W. B.; Congreve, D. N.; Brown, P. R.; Scherer, J. M.; Bischof, T. S.; Wu, M.; Geva, N.; Welborn, M.; Voorhis, T. V.; et al. Energy Harvesting of Non-Emissive Triplet Excitons in Tetracene by Emissive PbS Nanocrystals. *Nat Mater* **2014**, *13* (11), 1039–1043.

(31) Bell, R. P. The Theory of Reactions Involving Proton Transfers. *Proc R Soc Lond A* **1936**, *154* (882), 414–429.
(32) Evans, M. G.; Polanyi, M. Inertia and Driving Force of Chemical Reactions. *Trans. Faraday Soc.* **1938**, *34* (0), 11–24.
(33) Moreels, I.; Lambert, K.; Smeets, D.; De Muynck, D.; Nollet, T.; Martins, J. C.; Vanhaecke, F.; Vantomme, A.; Delerue, C.; Allan, G.; et al. Size-Dependent Optical Properties of Colloidal PbS Quantum Dots. *ACS Nano* **2009**, *3* (10), 3023–3030.
(34) Förster, T. Zwischenmolekulare Energiewanderung Und Fluoreszenz. *Ann. Phys.* **1948**, *437* (1–2), 55–75.

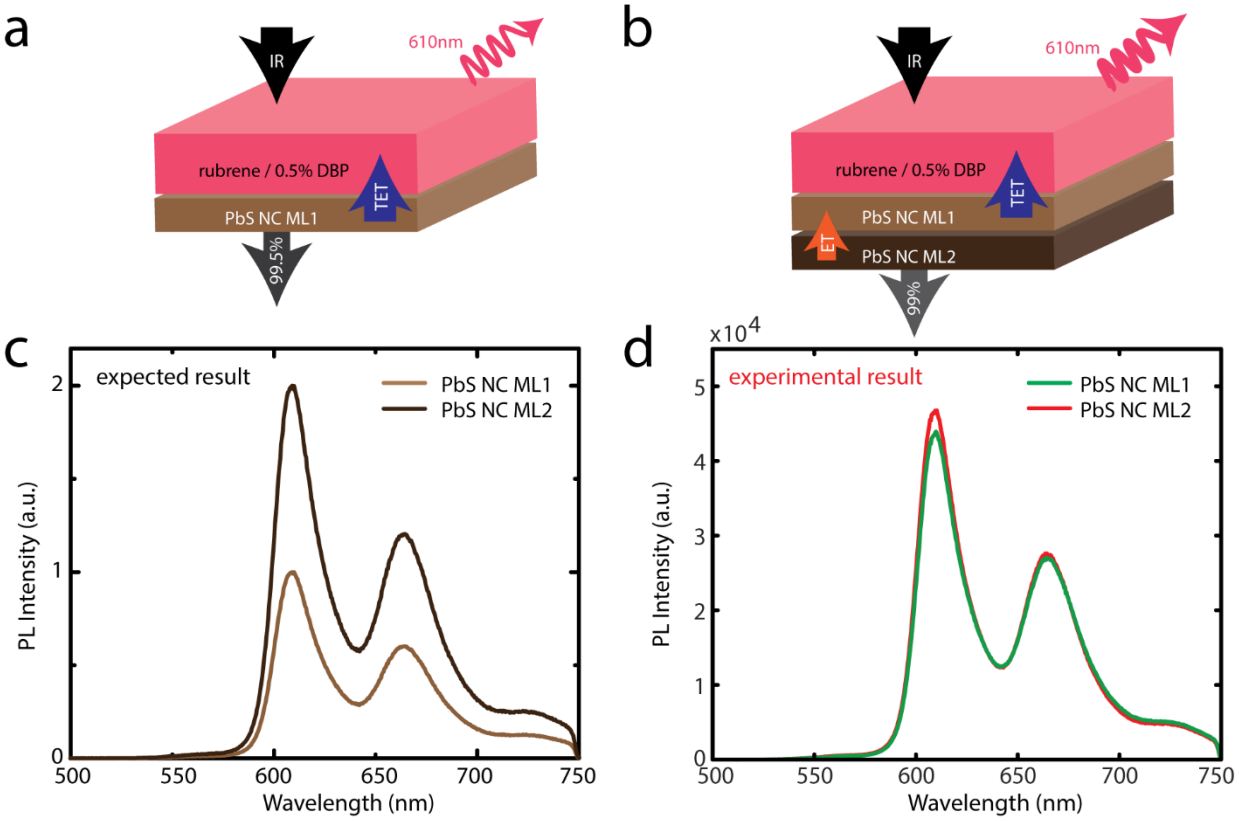

Figure 1: (a) Energy flow of the previously studied single PbS NC ML device. The PbS NCs are quenched via TET to the rubrene layer. Only ca. 0.5% of the incident photons are absorbed, while the other 99.5% pass through the device. (b) First-order approximation: to increase the absorbed photons by a factor of two, a second PbS NC ML is added. ET from the second ML to the first allows for subsequent TET to the rubrene. (c) Expected result of the steady-state upconverted light output from the dopant dye DBP (corresponding to the external upconversion efficiency), where two MLs of PbS NCs results in twice as much light output. (d) Experimental result, showing that an additional ML of NCs does not show a noticeable increase in the obtained upconverted light intensity, indicating a reduction of the internal upconversion efficiency by a factor of two.

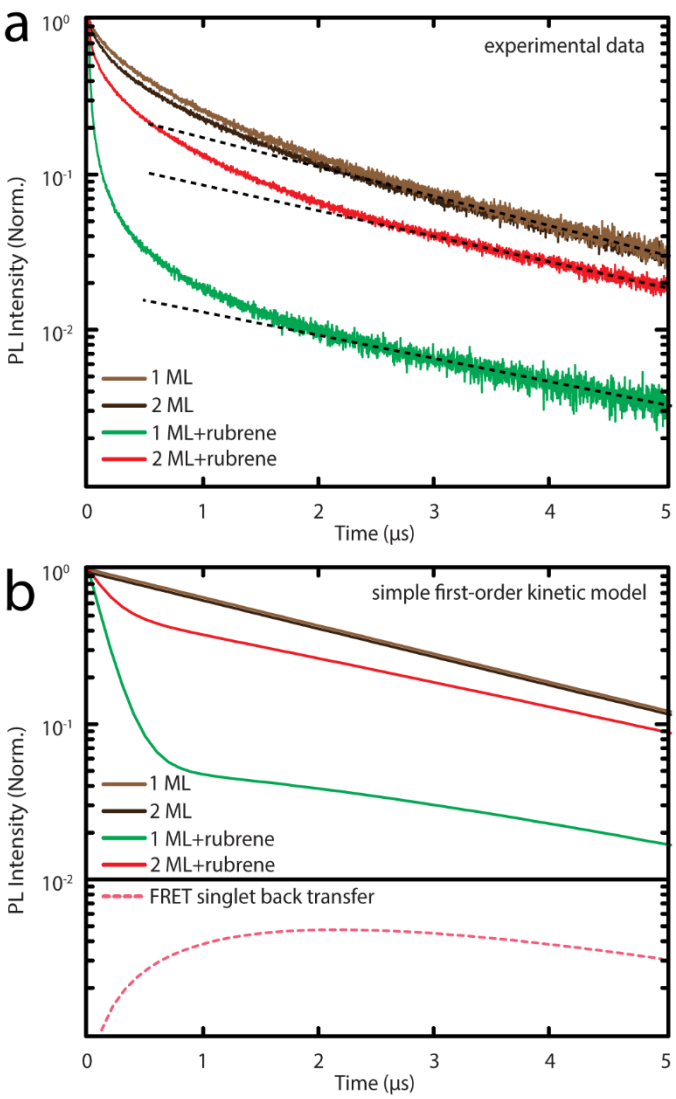

Figure 2: (a) Experimental PL dynamics of the one ML (two MLs) PbS film in light brown (dark brown) in absence of rubrene. In the presence of rubrene, the infrared PL dynamics of the PbS NC ML (two MLs) are quenched by TET to the triplet state of rubrene, shown in green (red). The non-parallelity of the late-time decay dynamics is highlighted by the dashed black lines, which function as guides to the eye. (b) Simple first-order kinetic model. The PbS decay dynamics are simulated as a monoexponential decay (brown) with a lifetime of 2.4 μs. In presence of rubrene, 92% (49%) of the population of one (two) ML PbS NCs is quenched on a 150 ns time-scale. To account for the late-time mismatch of the PL dynamics, singlet back transfer is modeled as a rising exponential with a 15 μs lifetime, convoluted with the 2.4 μs lifetime of the NCs (bottom inset).

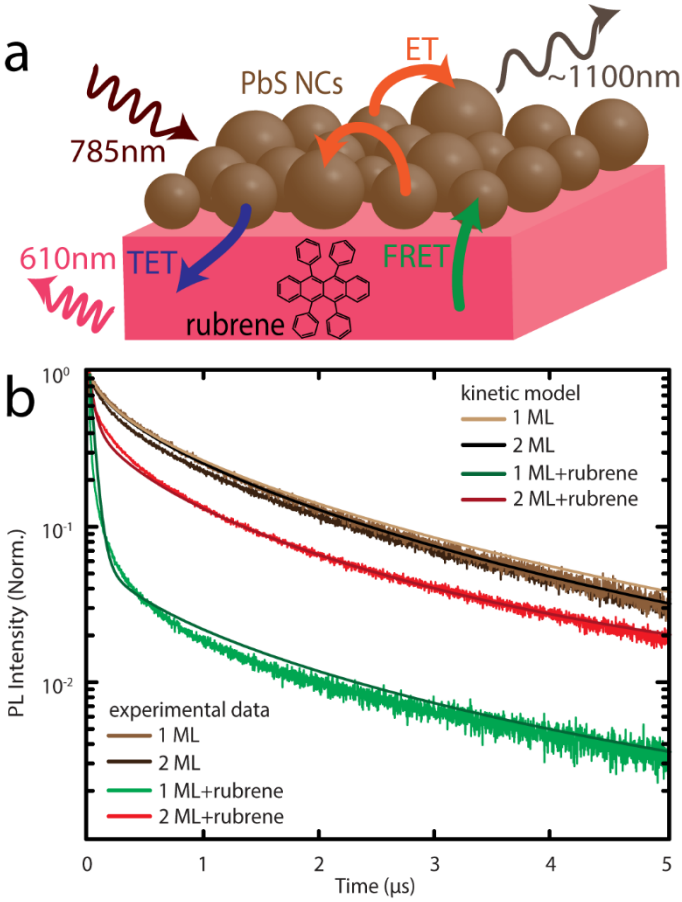

Figure 3: (a) An illustration of the system and the various rates considered in the model. The PbS NCs are excited at 785 nm. They can undergo inter-dot energy transfer or TET into rubrene. After TTA, the resulting singlets can emit, be far-field reabsorbed, or undergo FRET back into the sensitization layer. (b) Experimental PL traces for one and two NC MLs, in presence (green, red) and in absence of rubrene (light and dark brown). The fits obtained by the kinetic model are overlaid as solid lines. The model can capture the "bendiness" of the PbS NC PL dynamics stemming from energetic disorder very well.

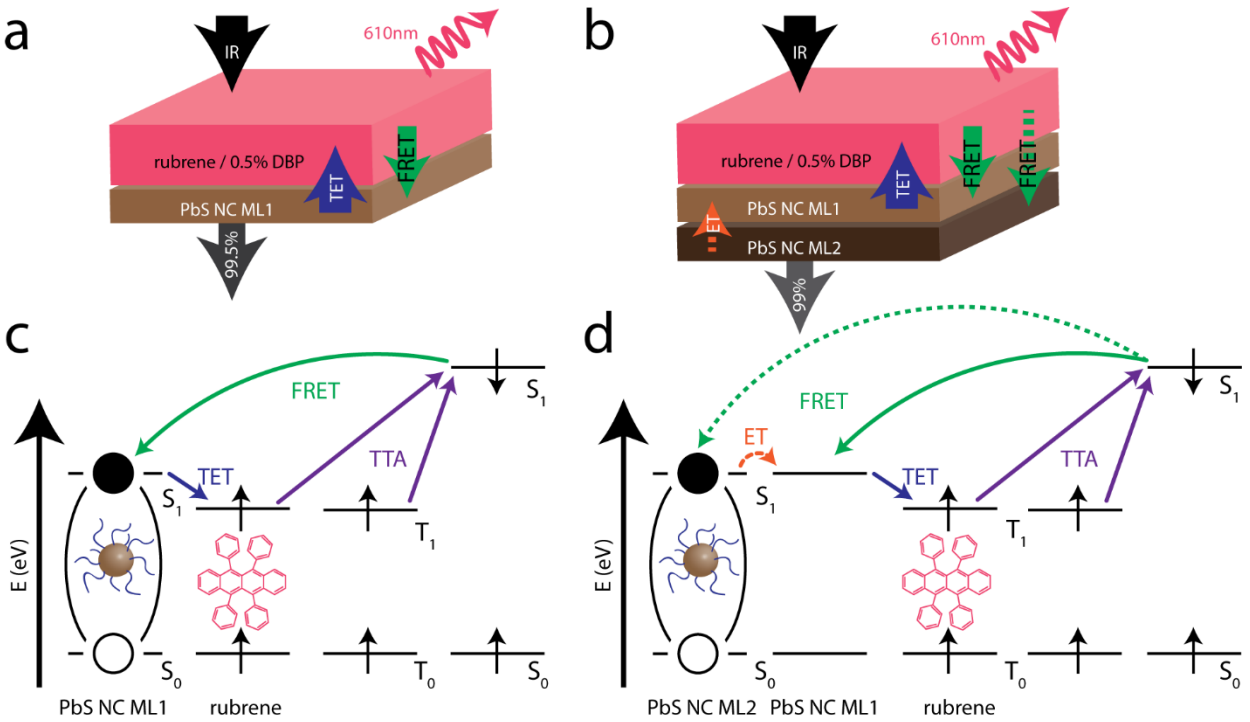

Figure 4: The flow of energy in the system. (a) The first PbS ML of NCs can readily transfer to rubrene, while accepting the singlets created by TTA back *via* FRET, which in turn can be recycled and transferred to rubrene again. (b) The first ML has similar properties as seen in (a). The second PbS ML however, undergoes inefficient ET to the first ML, and cannot undergo short-range TET to rubrene. It can still accept singlets created by TTA *via* long-range FRET, yet these are not recycled efficiently as in the case of 1 ML. The end result is an increase in the loss channels for little gain. (c, d) Energy level diagrams showing the energy transfer pathways for one and 2 ML upconversion devices. The additional fast (100ps) FRET step from rubrene to DBP has been omitted for simplicity.